

International Conference on Space Optics—ICSO 2014

La Caleta, Tenerife, Canary Islands

7–10 October 2014

Edited by Zoran Sodnik, Bruno Cugny, and Nikos Karafolas



Performance modelling of miniaturized flash-imaging lidars for future mars exploration missions

V. Mitev

A. Pollini

J. Haesler

João Pereira do Carmo



International Conference on Space Optics — ICSO 2014, edited by Zoran Sodnik, Nikos Karafolas, Bruno Cugny, Proc. of SPIE Vol. 10563, 105633C · © 2014 ESA and CNES
CCC code: 0277-786X/17/\$18 · doi: 10.1117/12.2304242

PERFORMANCE MODELLING OF MINIATURIZED FLASH-IMAGING LIDARS FOR FUTURE MARS EXPLORATION MISSIONS

V. Mitev¹, A. Pollini¹, J. Haesler¹, João Pereira do Carmo²
¹CSEM, Switzerland. ²ESA-ESTEC, The Netherlands

I. INTRODUCTION

Future planetary exploration missions require the support of 3D vision in the GN&C during key spacecraft's proximity phases, namely: i) spacecraft precision and soft Landing on the planet's surface; ii) Rendezvous and Docking (RVD) between a Sample Canister (SC) and an orbiter spacecraft; iii) Rover Navigation (RN) on planetary surface. The imaging LiDARs are among the best candidate for such tasks [1-3]. The combination of measurement requirements and environmental conditions seems to find its optimum in the flash 3D LiDAR architecture. Here we present key steps is the evaluation of novelty light detectors and MOEMS (Micro-Opto-Electro-Mechanical Systems) technologies with respect to LiDAR system performance and miniaturization. The objectives of the project MILS (Miniaturized Imaging LiDAR System, Phase 1) concentrated on the evaluation of novel detection and scanning technologies for the miniaturization of 3D LiDARs intended for planetary mission. Preliminary designs for an elegant breadboard (EBB) for the three tasks stated above (Landing, RVD and RN) were proposed, based on results obtained with a numerical model developed in the project and providing the performances evaluation of imaging LiDARs.

II. THE MODEL

The task of the numerical performance evaluation model in the MILS (Miniature Imaging LiDAR System) design is illustrated in Fig. 1. The figure of merit for the LiDAR performance is the overall range uncertainty per pixel for the required angular or horizontal resolution. The overall range uncertainty is defined as the statistical error plus the drift of the platform during the signal accumulation time and for a given horizontal (angular) resolution. The model takes as inputs the subsystems specifications and the environmental conditions for measurements (albedo, optical background). The allowed mass and power consumption determine the laser type and its power (pulse energy). The result from the calculation is the figure of merit. The next step is to compare the obtained values with the required ones. If the obtained values comply with the requirements, the combination of the subsystems specifications, the ranging method and operation modes are selected for the MILS preliminary design. In case they are not compliant, another selection is needed for subsystems and specifications, ranging method and operation modes. It has to be noted that both the measurement requirements and mass, and power consumption budget are top level inputs. The allowed mass and power consumption determine the subsystems specifications, the laser type and power being the most critical ones.

In the MILS project, a Technology Demonstrator BreadBoard (TDBB) has been built, which allowed assessing the performances of the main components of the miniature imaging LiDAR. The results obtained with the TDBB were used to verify the model, thus justifying its application for the MILS EBB designs.

Based on the results from the TDBB tests reported in [4], the detection based on SPAD (Single-Photon Avalanche Diode) array was selected as optimal for all the above stated mission measurement scenarios. The ranging method is the direct Time-of-Flight (TOF), more precisely, the Time Correlated Single Photon Counting (TCSPC) [5].

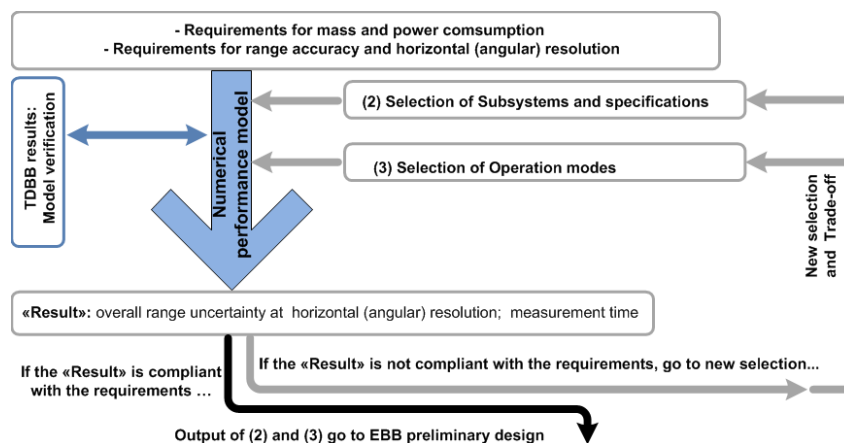


Fig. 1. The LiDAR numerical performance model in the context of MILS preliminary design

A. LiDAR signal and noise components

In Landing and RN the probed area is a Lambertian scattering surface filling entirely the single pixel footprint. In this case the detected backscattered signal in photon counts $N_S(r)$ at range r is determined as [6].

$$N_S(r) = E_L \frac{1}{E_{ph}} K_T K_R \eta \frac{A}{2\pi r^2} \rho \left(\frac{\Theta_p}{\Theta_0} \right)^2 \exp \left(-2 \int_0^r \alpha_{atm}(r') dr' \right) \quad (1)$$

E_L is the laser pulse energy; K_T and K_R are the efficiency of the transmitter and receiver, E_{ph} is the single photon energy, A is the receiver area, Θ_0 is the laser divergence assumed equal to the SPAD array Field-of-view; Θ_p is the FOV of the single pixel, η is the quantum efficiency and ρ is the Lambertian scattering albedo. The expression in the exponent is presented in scenarios with planet's atmosphere. It gives the two-ways atmospheric transmission factor, where α_{atm} is the extinction coefficient of the atmosphere.

In such case, the signal arriving from the atmosphere before the surface is modelled as [7]:

$$N_{atm}(r) = E_L \frac{t_{gate}}{E_{ph}} K_T K_R \eta \frac{A}{r^2} \frac{c \Delta r}{4\pi} \left(\frac{\Theta_p}{\Theta_0} \right)^2 \beta(r) \exp \left(-2 \int_0^r \alpha_{atm}(r') dr' \right) \quad (2)$$

Here $\beta(r)$ is the backscatter of the atmosphere at angle π in $(\text{m}^2 \text{sterad})^{-1}$; Δr is the length of the volume from which the atmospheric backscatter photons arrive, c is the velocity of light.

The ambient background signal is modelled as:

$$N_{bg} = S K_R \eta A \Theta_p^2 \rho \frac{1}{E_{ph}} B_F t_{gate} (\cos \varphi) (\cos \gamma) \quad (3)$$

Here S is the solar irradiance, B_F is the optical filter full width at half-maximum (FWHM); φ and γ are the solar zenith angle and the angle between the LiDAR beam and the normal to the surface. The dark electron number during the signal integration time shall be also added, is determined as $N_D = n_d t_{gate}$ where n_d is the dark count rate in number/sec⁻¹. Then the expectation value of the total noise photoelectron numbers is

$$N_{total_n}(r) = N_{atm}(r) + N_D + N_{bg} \quad (4)$$

For Rendezvous and Docking (RVD) the surface of the Space Canister (SC) is covered with retroreflectors and the backreflected laser light determines the received signal. The angular dimensions of the SC are lower than the angular resolution of the single pixel, i.e., the SC is seen in a single SPAD pixel. We use the expression for the backreflected signal from [8, 9].

$$N_S(r) = E_L \frac{1}{E_{ph}} K_T K_R \eta \frac{s_R A}{(\pi \Theta_0 r^2)^2} \quad (5)$$

The value s_R is the surface of the retroreflector. The dependence on r is at fourth power, which is different from the case for Landing and Rover Navigation. As the angular dimension of the probed object is less than the single-pixel angular resolution, the diffuse component of the backscatter signal shall be also expressed with the "range-at-fourth power" dependence [6], where s_D is the diffuse scattering surface of the SC.

$$N_{sd}(r) = E_L \frac{1}{E_{ph}} K_T K_R \eta \frac{s_D A}{r^4} \quad (6)$$

Thus, the expectation value of the total number of counts is

$$N_{total_c}(r) = N_s(r) + N_{atm}(r) + N_D + N_{bg} = N_s(r) + N_{total_n} \quad (7)$$

B. Signal-to-Noise Ratio and statistical range error

The Poisson probability distribution is expressed as $PD(k) = n^k \exp(-n) / k!$. Here n is the expected (mean) value and k is the realized value. In case of single photon detection k may take values only “1” or “0”. The expected values for signal and noise counts in the different scenario are given by eqs. (1-6). The probabilities for detection of “0” and “1” noise photoelectron are respectively:

$$p(total_noise_0) = (N_{total_n}(r))^k \exp(-N_{total_n}(r)) / 0! \quad (8)$$

$$p(total_noise_1) = [1 - p(total_noise_0)] \quad (9)$$

The probability to detect signal “0” and “1” is respectively

$$p(signal_0) = (N_s(r))^k \exp(-N_s(r)) / 0! \quad (10)$$

$$p(signal_1) = [1 - p(signal_0)] * p(total_noise_0) \quad (11)$$

The probabilities in (7-10) depend on the range from the LiDAR to the surface via the respective dependence of the signals and noises in eqs. (1-6).

The *SNR* is defined from the signal expectation value $Ex(signal)$ and the total noise variance $VAR(total_counts)$ as

$$SNR = \frac{Ex(signal_counts)}{\sqrt{VAR(total_counts)}} \quad (12)$$

The values for the signal expectation value and total noise variance, necessary for Signal-to-Noise (*SNR*) evaluation, are expressed below.

$$VAR(total_counts) = VAR(signal) + VAR(total_noise) \quad (13)$$

$$Ex(signal_counts) = p(signal_0) * 0 + p(signal_1) * 1 = p(signal_1) \quad (14)$$

$$VAR(signal_counts) = p(signal_1) * p(signal_0) \quad (15)$$

$$VAR(total_counts) = p(total_noise_1) * p(total_noise_0) \quad (16)$$

From (12-15) we may obtain the *SNR*

$$SNR = \frac{p(signal_1)}{\sqrt{p(signal_1) * p(signal_0) + p(total_noise_1) * p(total_noise_0)}} \quad (17)$$

The statistical range error $\sigma_R(r)$ is determined following the approach from [10], where we add a term responsible for the contribution of the random jitter of the response time in case of SPAD detection.

$$\sigma_R(r) = \sqrt{\left[\left(\frac{c\tau_L}{2} \frac{1.2}{SNR(r)} \right)^2 + \left(\frac{c\tau_{spad}}{2(NDC(r))} \right)^2 + \left(\frac{c\tau_c}{2} \right)^2 \right]} \quad (18)$$

In (17), τ_L is the laser pulse duration defined for a Gaussian pulse shape, τ_c is the resolution of the TDC, τ_{spad} is the SPAD response time jitter, *NDC* is the number of the detected counts. The statistical range error is a function on the range of probing via *SNR*, i.e., the received signal and the noises, and *NDC*.

III. PRELIMINARY DESIGN, KEY COMPONENTS AND LAYOUT

The layouts for the preliminary MILS designs are presented for Landing, RVD and RN applications in Fig. 1.

As the SPAD array is the key technology for the perspective MILS, one of our goals was to assume the same specifications of this component for all applications. The critical specification of the SPAD array, necessary for the realisation of the proposed MILS designs, is the pixel number, 1024x1024 pixels. Presently there is still no such developed component, but there are no technological limitation for its design and realisation. Another critical and common requirement is the microlens array for increasing the fill factor from the current $\sim 1\%$ to a fill factor of $\sim 70\%$. As it appeared from the model study, the MOEMS is needed for MILS RVD only. The specifications for SPAD array and MOEMS are listed in Table 1.

The lasers in MILS for all three applications are pulsed but of different types. Their specifications are presented in Table 2. Table 3 presents the specifications of the selected MILS receiver optics.

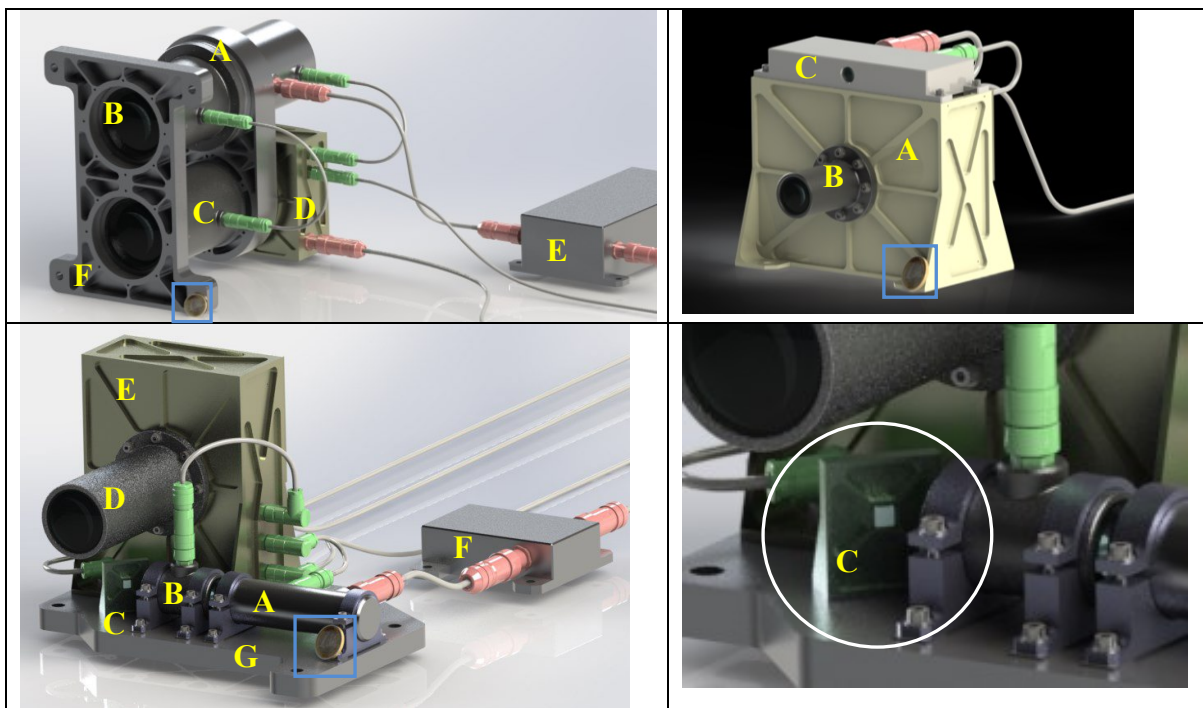


Fig. 1. Proposed MILS layout. **Top-Left:** Landing; (A) Laser; (B) Transmitter; (C) Optical receiver; (D) Detector and processor; (E) Laser power supply; (F) Optical bench; **Bottom-Left:** RVD; (A) Laser; (B) Transmitter; (C) MEMS for slow scanning; (D) Optical receiver; (E) Detector and processor; (F) Laser power supply; (G) Optical bench; **Top-Right:** RN. (A) Detector; (B) Optical receiver; (C) Laser and Laser power supply; **Bottom-Right:** Zoom of RVD layout showing the MOEMS (in the circle). A coin of one Euro is put for size comparison inside the square.

Table 1. Specifications of the SPAD array and MOEMS required in MILS design

SPAD array specifications, all applications		MOEMS specifications, RVD only	
Quantum efficiency	>20% at 532 nm >15% at 635 nm	Mirror size	> 6 mm x 4 mm
Pixel number	1024x1024	Wavelength	532 nm
Pixel pitch/size	50 μm / 5 μm	Angular step (optical)	2 deg
Dark count rate	<1000 cps per pixel	Angular expand (optical)	+/- 10 deg
Dead time	<150 ns	Damage threshold	>130 kW/cm at laser pulse duration 1 ns
Jitter of response time	<150 ps	Single step time	≤ 0.1 s

Table 2. Specifications of the lasers selected in MILS design

Specification	Landing	RVD	RN
Laser Type	Q-switched, single giant pulse	Micropulsed, Nd:YAG, 2 nd harmonic	Diode laser, gain-switched
Wavelength	532nm	532nm	635nm
Pulse repetition rate (PRR)	1Hz	25KHz	Nominal: 1MHz Burst: 80MHz
Pulse energy	Mars: >3mJ Moon: >12mJ	>3μJ	125nJ
Pulse duration	<1ns	<1ns	<70ps
Beam profile after the transmitter	Top-flat	Top-flat	Top-flat
Maximum allocated consumed power	30W	22.5W	11.25W

Table 3. Specifications of the receiver optics selected in MILS design

Specification	Applications:		
	Landing	RVD	RN
Aperture	Diameter 80mm	Diameter 40mm	Diam. 50mm
Focal length:	From 400mm to 225mm	140mm	140mm
Optical transmission without IF	> 0.7	>0.7	> 0.7
IF, FWHM	1.5nm	1.5nm	5nm
IF, transmission	>0.55	>0.55	>0.75

III. RESULTS FROM PERFORMANCE MODELLING OF THE PROPOSED DESIGNS

A. MILS for Landing

The high landing velocity of the space craft determines a large added component to the overall uncertainty, if the LiDAR measurement is performed by the traditional TCSPC approach of histogram based on combining counts from multiple laser pulses. To avoid this issue we propose to build a histogram of counts arrivals from one laser pulse and from all pixels. The laser pulse shall have sufficiently high energy, so the expectation value of the signal counts is more than 1, respectively the probability for signal count detection is close to 1. In such case the peak of the histogram defines the average range to surface and the width of the peak provides a selection of the signal counts out of the noise and atmospheric ones. The consumed laser power is determined by the “stand-by” and “pulsing” power consumption, where the latter may be small for a few pulses per second.

We have to note that in probing with expectation values of the signal counts being more than 1, the effect of photon pileup [11] takes place. A treatment following the model proposed in [5] showed that the systematic error does not exceed half of the range corresponding to the laser pulse duration as TOF. In our case (see Table 2) this value is in the order of ~7.5cm and affects in the same way all pixels. Thus this effect does not distort the 3D image and may not be taken into account.

In Fig. 2 we present the results of one example of Landing on Mars, imaging of the surface taking place when the SC is at altitude between 1000m and 200m. The evaluation of the vertical accuracy is presented, together with the horizontal ground resolution. The values are calculated for two cases: without pixel binning and with 3x3 pixels binning. Without pixel binning the resolution is less than 0.14m for all ranges, while for the case of pixel binning it is less than 0.3m for all ranges. The specified ground resolution for this case is less than 0.3m, i.e., in both operation modes the MILS design satisfy this requirement. The statistical range uncertainty is not specified for this case in the requirements of the study. The result shows that without pixel binning statistical

range uncertainty varies from 0.05m at 200m to 0.5m at 1000m, while with pixel binning it varies from 0.02m at 200m to 0.18m at 1000m. The presented result shows also that pixel binning may be used to trade-off horizontal ground resolution versus range uncertainty during different descent stages.

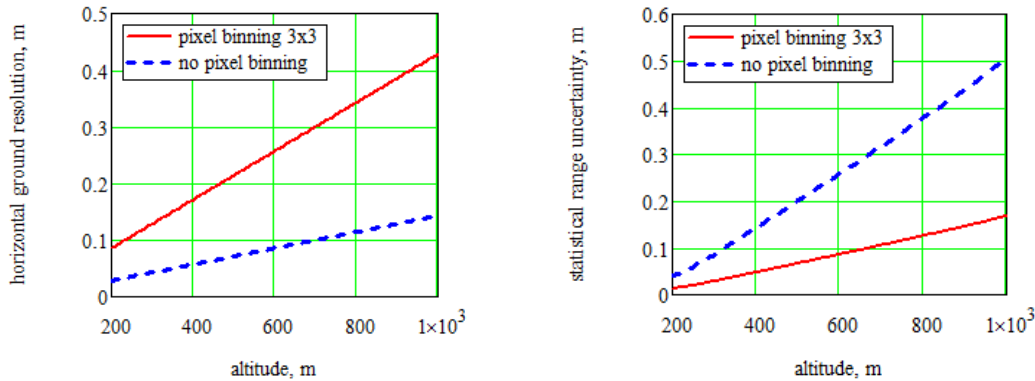


Fig. 2. Landing on Mars, Imaging from . **Left:** Horizontal ground resolution. **Right:** Statistical range uncertainty.

B. MILS for RVD

Due to the fact that in RVD scenario the SC occupies only one of the pixels of the SPAD array, we cannot use probing with single laser pulses and combining the counts from all pixels in one histogram. The laser shall be with high repetition rate and respectively low pulse energy (Table 3).

The MOEMS is used to implement two operation modes: acquisition and tracking. The FOV of the LiDAR is defined by the full area of the SPAD array and covers 20x20deg. The laser beam divergence is sufficient to cover a segment of 2x2deg in the LiDAR FOV. The beam is pointed successively by MOEMS to each of the 2x2deg segments until it probes the overall LiDAR FOV. This procedure defines the acquisition mode. After the SC is identified in one of the 2x2deg segments, the MOEMS is used to follow it, defining the tracking mode. The required angular resolution in the study is for RVD is 0.05deg. Thus, it may be achieved with a SPAD array having less pixel numbers than in Table 3, anyhow, the redundant pixels give the possibility for improving the range accuracy versus the angular resolution at very short ranges, where the SC image occupies some number of pixels in the array.

Fig. 3 presents the overall range uncertainty of MILS measurement, defined as the sum of the statistical error and the uncertainty from the relative spacecraft velocity. As we see, the selected design and operation modes fulfill the requirement for range uncertainty for all ranges. The calculations are performed with the decrease of the signal integration time and increase of the laser beam divergence, with the decrease of the distance between the orbiter and the SC. This decrease of the integration time and increase of the beam divergence are assumed as stepwise functions, what results on also stepwise decrease of the overall range error.

C. MILS for RN

The requirements for MILS range accuracy in RN are: (i) better than 10 cm for the ranges 10m – 100m (regional); better than 3cm for ranges 4m – 10m (midrange); better than 1cm for ranges less than 4m (local). The 3D LiDAR imaging is performed when the Rover is not moving. Thus, the overall uncertainty is determined only by the statistical uncertainty. We propose to use in this case gain-switched diode laser having pulse duration of 100ps or less. This type of laser gives the advantage to use two operational modes, called “nominal” and “burst”.

In the nominal mode the laser PRR is such that the ambiguity range is much larger than the range to the probed surface, specified as max 100m. With such PRR the specified range accuracy cannot be reached, but its accuracy defines a range window where the probed surface is located. In the burst mode the PRR is high and the ambiguity range is shorter than the range to the probed surface. With the condition that the ambiguity range in burst mode is larger than the range accuracy in nominal mode, the measurement in nominal mode selects the range window where the multiple LiDAR echo from the burst mode indicates the precise range.

In addition, for regional navigation it is necessary to use pixel binning for additional augmentation of the accuracy. That is why in the case of RN we select a SPAD array with a number of pixels (see Table 3) larger than required by the specified angular resolution for RN 0.5x0.5deg, where the single measurement FOV of the instrument without rotation of its platform (pan and tilt) is ~20x20deg.

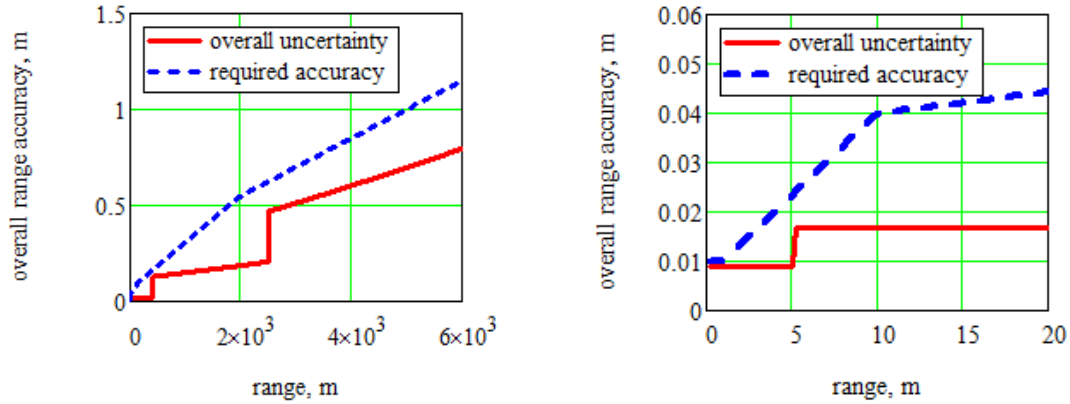


Fig.3. Overall uncertainty for MILS RVD. The blue line presents the required uncertainty; **Left:** All ranges; **Right:** Short ranges only.

The results from the statistical range uncertainty are presented in Fig. 4. As we see, the combination of burst mode and pixel binning are sufficient to obtain the required accuracy (10 cm) at all ranges, while below ~45m the nominal range with pixel binning is also sufficient. The range accuracy requirement (3 cm) for midrange navigation may be fulfilled without pixel binning but it requires burst mode. In this case the redundant pixel number will provide angular resolution better than the specified one. The results for local navigation are not presented here. Anyway, they show that the requirements may be fulfilled with burst mode and no pixel binning.

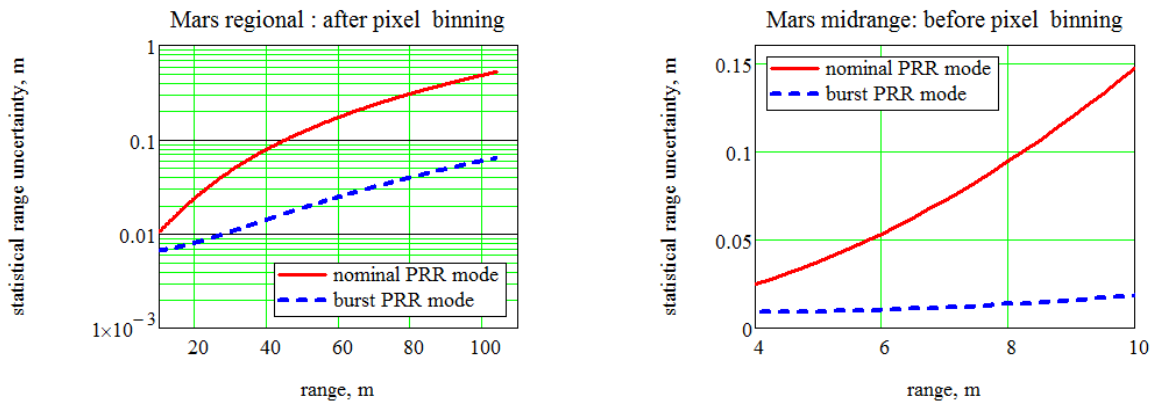


Fig. 4. MILS for Rover Navigation on Mars, dependence of the statistical uncertainty on the range. The “statistical range uncertainty” is equivalent to “range accuracy”. **Left:** regional mode with pixel binning 24x24; **Right:** midrange mode without pixel binning.

IV. CONCLUSION

The most promising technologies having the potential for miniaturization of the Imaging LiDAR have been identified, reviewed and experimentally investigated in [4]. The results from the technology evaluation have been used to validate the two components of the LiDAR numerical simulation model for the selected approach of SPAD array detection: i) the power balance or LiDAR equation; (ii) the dependence of the statistical range error on the signal and the noise, and on the system parameters.

The LiDAR architecture and the sensor technology for the realization of the perspective MILS were selected, following the mission requirements. The validated MILS numerical evaluation model was used to prove that the performances for the proposed preliminary designs may meet the requirements in each of the required proximity navigation scenario: Landing, RVD and RN.

The critical specification of the SPAD array, necessary for the realisation of the proposed MILS designs, is the pixel number. All other specifications, as well as the specifications of MOEMS and the lasers, are in line with the state of the art. As for SPAD array, there is no technological limitation to reach such pixel-number increase and to implement the microlens array on the chip, necessary to augment the fill factor. There is also no technology obstacle for space qualification of the critical components.

ACKNOWLEDGEMENTS

Acknowledgements are due to all MILS partners, more specifically to Dr. T. Akiyama, Dr. W. Noell and Prof. N. de Rooij from EPFL, Switzerland, Dr. S. Lani from CSEM, Switzerland, D. Perenzoni and D. Stoppa from FBK, Italy, Ch. Kolleck from LZH, Germany, M. Chapuy, F. Capolupo and E. Kervendal from Astrium EADS, France.

REFERENCES

- [1] J. Pereira do Carmo, B. Moebius, M. Pfennigbauer, R. Bond, I. Bakalski, M. Foster, S. Bellis, M. Humphries, R. Fisackerly, B. Houdou, "Imaging lidars for space applications", *Proceedings of SPIE: Optics and Photonics*, vol. 7061-16, 2008.
- [2] A. E. Johnson, J. A. Keim, T. Ivanov "Analysis of Flash Lidar Field Test Data for Safe Lunar Landing" *IEEE Aerospace Conference, 06 - 13 March 2010, Big Sky MT, USA, Proceedings*, pp. 135-145, 2010.
- [3] J. D. Weinberg, R. Craig, P. Earhart, I. Gravseth, K. L. Miller, "Flash LIDAR Systems for Hazard Detection, Surface Navigation and Autonomous Rendezvous and Docking", *LEAG Workshop on Enabling Exploration: The Lunar Outpost and Beyond, October 1-5, 2007, Houston, Texas*, pp.3023-3024, 2007.
- [4] A. Pollini, J. Haesler, V. Mitev, João Pereira do Carmo, et al. "Evaluation of Novel Technologies for the miniaturization of Flash Imaging LiDAR", *paper Ref. 66403, ICSO 2014, 7-10 October, Tenerife, Canary Islands, Spain*, to be published, 2014.
- [5] C. Niclass, "Single-Photon Imaging in CMOS: Picosecond Resolution for Three-Dimensional Imaging", *PhD Thesis, EPFL, Lausanne* 2008.
- [6] A. V. Jelalian, *Laser Radar System*, Artech House, Boston-London, 1992.
- [7] R. M. Measures. *Laser remote sensing, fundamentals and applications*, John Wiley&Sons, 1984
- [8] J. J. Degnan, J. J., 1993, "Millimeter Accuracy Satellite Laser Ranging: A Review"; in *Smith, D. E., and D. L. Turcotte (Eds.) "Contributions of Space Geodesy to Geodynamics: Technology", Geodyn. Ser.*, vol. 25, 213 pp., doi:10.1029/GD025, AGU, Washington, D. C.. pp. 133-162, 1993.
- [9] I. Makram, M. Afaf, A. El-Hameed and G. F. Attia, "Analytical Studies of Laser Parameters for Ranging and Illuminating Satellites from H-SLR Station". *Space Research Journal*, vol. 4, pp. 71-78, 2011.
- [10] D. C. Carmer and L. M. Peterson, "Laser radar in robotics", *Proc. of the IEEE*, vol. 84, 299-320, 1996.